ELSEVIER

Contents lists available at ScienceDirect

Environmental Research

journal homepage: www.elsevier.com/locate/envres





Photosynthetic microbial fuel cells for methanol treatment using graphene electrodes

Kalimuthu Jawaharraj ^{a, c, f, g}, Pawan Sigdel ^{a, f}, Zhengrong Gu ^{d, f}, Govarthanan Muthusamy ^{e, h}, Rajesh Kumar Sani ^{b, c, f, g}, Venkataramana Gadhamshetty ^{a, c, f, g, *}

- ^a Civil and Environmental Engineering, South Dakota Mines, 501 E. St. Joseph Street, Rapid City, SD, 57701, USA
- ^b Chemical and Biological Engineering, South Dakota Mines, 501 E. St. Joseph Street, Rapid City, SD, 57701, USA
- ^c BuG ReMeDEE Consortia, South Dakota Mines, 501 E. St. Joseph Street, Rapid City, SD, 57701, USA
- d Agricultural and Biosystems Engineering, South Dakota State University, 2100 University Station, Brookings, SD, 57701, USA
- ^e Department of Environmental Engineering, Kyungpook National University, Daegu, South Korea, 80 Daehak-ro, Buk-gu, Daegu, South Korea
- ^f 2D-materials for Biofilm Engineering, Science and Technology (2DBEST) Center, South Dakota Mines, 501 E. St. Joseph Street, Rapid City, SD, 57701, USA
- g Data-Driven Materials Discovery for Bioengineering Innovation Center, South Dakota Mines, 501 E. St. Joseph Street, Rapid City, SD, 57701, USA
- h Department of Biomaterials, Saveetha Dental College and Hospital, Saveetha Institute of Medical and Technical Sciences, Chennai, 600 077, Tamil Nadu, India

ARTICLE INFO

Keywords: Graphene Methanol Rhodobacter Photosynthetic Microbial fuel cells

ABSTRACT

Photosynthetic microbial fuel cells (pMFC) represent a promising approach for treating methanol (CH₃OH) wastewater. However, their use is constrained by a lack of knowledge on the extracellular electron transfer capabilities of photosynthetic methylotrophs, especially when coupled with metal electrodes. This study assessed the CH₃OH oxidation capabilities of *Rhodobacter sphaeroides* 2.4.1 in two-compartment pMFCs. A 3D nickel (Ni) foam modified with plasma-grown graphene (Gr) was used as an anode, nitrate mineral salts media (NMS) supplemented with 0.1% CH₃OH as anolyte, carbon brush as cathode, and 50 mM ferricyanide as catholyte. Two simultaneous pMFCs that used bare Ni foam and carbon felt served as controls. The Ni/Gr electrode registered a two-fold lower charge transfer resistance $(0.005 \ k\Omega \ cm^2)$ and correspondingly 16-fold higher power density (141 mW/m²) compared to controls. The underlying reasons for the enhanced performance of *R. sphaeroides* at the graphene interface were discerned. The real-time polymerase chain reaction (PCR) analysis revealed the upregulation of cytochrome *c* oxidase, aa3 type, subunit I gene, and Flp pilus assembly protein genes in the sessile cells compared to their planktonic counterparts. The key EET pathways used for sustaining CH₃OH oxidation were discussed.

1. Introduction

The market value of the wastewater industry has been projected to reach as high as \$ 263 billion by 2028 (Statista, 2022). This projection takes into account the challenges to treat industrially relevant recalcitrant wastewaters containing CH₃OH. Such wastewater discharges are typical in industries involved in the production of oil and gas (Yamamuro et al., 2014), esters, formaldehyde, and other chemicals (Langrand et al., 1990; Y et al., 1987). Being a volatile organic compound, CH₃OH from wastewater tends to escape into the atmosphere where it displays abundance and extended lifetime (Cai et al., 2021). Also, the discharge limit for CH₃OH has been restricted to 44,000 tons/year. This limit is particularly true for industries that contribute to 70% of the total

hazardous air pollutants (EPA, 2004, 1998). The potential health impacts due to CH₃OH include nerve damage, cancer, and respiratory illness (EPA, 1998). There is an urgent need to develop innovative bioprocesses for the targeted treatment of CH₃OH (Swain and Somerville, 1978). Although the conventional treatment processes including the activated sludge process can treat CH₃OH, it requires significant energy inputs.

Earlier studies (Choudhury et al., 2017; Pant et al., 2010) demonstrated the use of MFCs and microbial capacitive deionization cells for treating produced water containing high levels of CH₃OH (Shrestha et al., 2018). The half cell oxidation reaction for CH₃OH (Eq (1)) can be thermodynamically coupled with half cell reduction reaction for soluble electron acceptors based on nitrate (Eq (2)) and sulfate (Eq (3))

^{*} Corresponding author. Department of Civil and Environmental Engineering. South Dakota Mines. 501 E St Joseph St, Rapid City, SD, 57701, USA. *E-mail address:* Venkata.Gadhamshetty@sdsmt.edu (V. Gadhamshetty).

(Tchobanoglus et al., 2003).

Electron donor:

$$\frac{1}{6}CH_3OH + \frac{1}{6}H_2O \rightarrow \frac{1}{6}CO_2 + H^+
+ e^- \left(\Delta G^o = -37.51 \frac{\text{kJ}}{\text{electron equivalent}}\right)$$
(1)

Electron acceptor:

$$\frac{1}{5}NO_{3}^{-} + \frac{6}{5}H^{+} + e^{-} \to \frac{1}{10}N_{2}
+ \frac{3}{5}H_{2}O \quad \left(\Delta G^{o} = -71.67 \frac{kJ}{\text{electron equivalent}}\right)$$
(2)

$$\frac{1}{8}SO_4^{2-} + \frac{19}{16}H^+ + e^- \to \frac{1}{16}H_2S + \frac{1}{16}HS^-
+ \frac{1}{2}H_2O \quad \left(\Delta G^{\circ} = 21.27 \frac{kJ}{\text{electron equivalent}}\right)$$
(3)

Coupling CH₃OH oxidation with nitrate reduction yields -109.18 kJ/electron equivalent and that with sulfate reduction yield -16.24 kJ/ electron equivalent. These negative values indicate that the CH3OH oxidation becomes spontaneous when coupled with suitable terminal electron acceptors. It is possible to develop biocatalysts that transfer electrons from the CH₃OH oxidation directly onto the anode in MFCs. Such biocatalysts were recently enriched using indigenous microorganisms from the produced water samples procured from hydraulically fractured Bakken shale. This consortium consisted of Actinobacteria, Bacteroidia, and γ-proteobacteria (Jawaharraj et al., 2020b). A significant fraction in this consortia consisted of R. sphaeroides (~29%) and others from β -proteobacteria, γ -proteobacteria, and Bacteroidia classes (Jawaharraj et al., 2020b). Such consortium can generate significant current output (220 mW m⁻²) using CH₃OH as the sole carbon source (Yamamuro et al., 2014). Our recent study suggested the use of R. sphaeroides for oxidizing CH₃OH in MFCs (Islam et al., 2020). Its performance was on par with classic methylotrophs including Methylococcus capsulatus Bath and Methylosinus trichosporium OB3b, respectively which yielded maximum power densities of 110 mW m⁻² and 205 mW m⁻² respectively (Jawaharraj et al., 2019, 2021).

Photosynthetic microorganisms such as *Rhodobacter capsulatus* (Mirza et al., 2022) and *Rhodobacter gluconicum* (Maddalwar et al., 2021) have been reported to serve as effective biocatalysts in MFCs. Owing to the available genome information, *R. sphaeroides* is evolving as a model organism for studying environmental biotechnology applications (e.g., generation of electricity, polyhydroxybutyrate, membrane protein, and hydrogen) (Cadirci, 2018; Jawaharraj et al., 2020a, 2020b; Wong et al., 2016). *Rhodobacter* sp. has also been reported to serve as anoxygenic phototrophic exoelectrogen that can use both organic carbons in wastewater (Qi et al., 2018) and CO₂ as carbon sources in MFCs (Li et al., 2021). *R. sphaeroides* cells can use CH₃OH as a carbon source, harvest energy from visible light, grow with minimal levels of oxygen (Cadirci, 2018), and thus serve as biocatalysts in pMFCs (Wilson et al., 2008).

The pMFC performance can be improved by using inexpensive metal electrodes (Huang et al., 2015) that offer structural stability, high electrical conductivity, tunable wettability, and desirable hierarchical pore structures. However, metals are prone to microbiologically influenced corrosion (Tripathi et al., 2021), which drives the leaching of toxic metal ions into the media and hampers cell growth (Yaqoob et al., 2020). This issue can be alleviated by modifying nickel with minimally invasive barrier coatings based on atomically thin graphene materials (Chilkoor et al., 2020, 2021; Krishnamurthy et al., 2013). Such graphene materials can also promote the bio-electrocatalytic activity of methylotrophs (Kaur et al., 2020; Huang et al., 2015). This study addresses knowledge gaps regarding the use of Ni/Gr electrodes for enhancing the bioelectrochemical interactions of *R. sphaeroides* fed with CH₃OH as the sole carbon source in pMFCs. This study also reveals the genomic

insights of R. sphaeroides biofilms exposed to nickel electrodes in pMFCs.

2. Materials and methods

2.1. Preparation and characterization of plasma exfoliated graphene on nickel (Ni/Gr)

Graphene electrodes were obtained by modifying Ni foams with an active mixture of plasma-exfoliated graphene (Gr) (80% w/w), acetylene black (10%), and polytetrafluoroethylene (10%). This mixture was pressed on a side of $1^{\prime\prime}$ x $1^{\prime\prime}$ Ni foam (EQ-bcnf-16 m, MTI Corp) with $1000~{\rm kg/cm^2}$ force for 10 min. The foam was dried for 12 h at 60 °C and used as an anode in pMFCs. Details on the graphene exfoliation procedures using a dielectric barrier discharge plasma are described elsewhere (Wang et al., 2017; Hummers Jr and Offeman, 1958). The contact angle and the wettability were assessed using a goniometer (Model 500, ramé-hart Instrument Co.). The contact angle was evaluated using a DROP-image advanced v2.4 software by dropping a single drop of sterile water.

2.2. Characterization of electrodes using Raman spectroscopy

Raman spectra of the electrodes were recorded using XploRA Plus Raman confocal microscope (Horiba Scientific) at room temperature. The spectra were taken with 532 nm excitation. A silicon (Si) wafer with a first-order phonon band of Si at 520 cm $^{-1}$ was used for calibration with zero-order correction of the used grating. The spectrograph is equipped with a SIN-EM FIUV CCD detector and grating of 600, 1200, 1800, and 2400 nm. The Raman spectra were taken using the grating of 1200 nm with a 100X magnification objective. The optimum signal-to-noise ratio was achieved by adjusting the acquisition time to 4–6 s with accumulated spectra of 2-3. The laser intensity was limited to 10 % to avoid any alterations to the sample. Four to five different randomized spots were measured for each sample. The spectra were then smoothened via LabSpec 6.6.2.7.

2.3. R. sphaeroides cultivation in pMFC

A pure culture of *R. sphaeroides* was cultured in NMS medium supplemented with 0.1% CH₃OH as a carbon source (Bowman and Sayler, 1994). The *R. sphaeroides* cultures were grown under shaking conditions (150 rpm) at 29 \pm 1 °C, and a pH of 6.8. The cell growth was monitored as absorbance at 600 nm using the EPOCH 2 microplate reader (BioTek). Pure cultures from the mid-exponential growth phase were used to inoculate pMFCs.

2.4. Electrochemical impedance spectroscopy (EIS) and cyclic voltammetry (CV)

R. sphaeroides cultures from the exponential growth phase were introduced as pure inocula (10% inoculum) in the anode compartment of an H-type batch pMFC. The R. sphaeroides cells in pMFC were incubated under photoheterotrophic mode by illuminating them at ~700 lux white light at 29 \pm 1 $^{\circ}$ C. Under the photoheterotrophic mode of growth, R. sphaeroides was made to use light as the source of energy and CH₃OH as the sole source of carbon. The test anode was Ni/Gr (surface area = 10 cm²) and controls were bare Ni (10 cm²) and CF (10 cm²). The cathodes were carbon brushes (130 cm²). The analyte consisted of 200 mL NMS media supplemented with 0.1% CH₃OH and catholyte of 100 mM potassium ferricyanide in phosphate buffer (50 mM, pH 7.0). A CMI-7000 cation exchange membrane (Membranes International Inc, USA) separated the two compartments. This strong acid cation exchange membrane comprises a polymer structure based on cross-linked divinylbenzene and gel polystyrene. This membrane was treated with 5% NaCl for 12 h to allow for expansion and hydration (Shrestha et al., 2016). The interelectrode spacing was limited to 0.005 m. Control MFCs were configured similarly except that they were devoid of CH₃OH.

All the pMFCs were operated with a load of 150 Ω . The voltage across the load was monitored continuously using a DAQ/54 module (I/O Tech Inc., Cleveland OH). The polarization curves and EIS profiles were generated every 5 days. The values of power and current were normalized to the surface area of the anode. EIS tests were performed at open-circuit conditions using a Reference 3000 potentiostat (Gamry Instrument Inc., PA). An alternating current signal (amplitude $=\pm 10$ mV) was used to get the EIS spectra in the frequency range of 10 kHz to 10 MHz. The counter sense and counter electrode were connected to the cathode and the working sense and working electrode were connected to the anode. EIS spectra were studied using both the Nyquist plots (real impedance vs. imaginary impedance) and the Bode plots (phase angle vs. frequency). EIS data were analyzed using the electrical equivalent circuit (EEC) fitting method (Fig. 3a inset). The EEC was based on a modified Randles circuit consisting of an ohmic resistance (R_{Ω}), polarization resistance (Rp) and Warburg diffusion impedance (W), and constant phase element (CPE). Reference 3000 potentiostat was used to run cyclic voltammetry (CV) with following parameters: equilibrium time-1000 s, scan rate - 10, 25 and 50 mV/s; $E_i - 1$ V vs Ag/AgCl; $E_f - 1$ V vs Ag/AgCl. CV tests were performed using CF or Ni/Gr as working electrode, carbon brush as cathode, and Ag/AgCl as a reference electrode. Kramer-Kronig compliant equivalent circuits were used to assess the reproducibility of impedance data.

2.5. Biofilm morphology analysis using scanning electron microscope (SEM)

The electroactive biofilms on the electrodes were washed gently with distilled water to remove the unbound planktonic cells. SEM was used to analyze the morphology of R. sphaeroides biofilm after fixing them using 3% glutaraldehyde in sodium cacodylate buffer (0.1 M, pH = 7.2) for 2 h at room temperature (Dedysh et al., 2015). The biofilm samples were then rinsed with sodium cacodylate buffer three times followed by rinsing in double-distilled water for five times. They were then dehydrated sequentially in 25%, 50%, 75%, and 100% acetone and dried overnight in a desiccator (Roy et al., 2012). Zeiss Supra40 SEM was used to analyze the three electrodes before and after the exposure to biofilms.

2.6. RNA extraction and complementary DNA synthesis

Planktonic cells of R. sphaeroides from the anode compartment of pMFCs were harvested after 5 days and centrifuged at 10,000 rpm at 4 °C for 15 min. The cells were transferred to tubes that were transferred to ice immediately and stored at -80 °C. The R. sphaeroides biofilms formed on the anode surface were washed gently with a phosphatebuffered saline (pH = 6.5) and then scraped using the nuclease-free spatula before transferring to pre-chilled centrifuge tubes. RNA was extracted from the frozen cells using a TRIzolTM MaxTM Bacterial RNA Isolation Kit (Ambion, Life Technologies, USA) using the manufacturer's protocol. The total RNA was treated with double-stranded DNase (dsDNase) for 2 min at 37 °C to remove the genomic DNA contamination. The purity of treated RNA was quantified using a Nanodrop 1000 spectrophotometer (Thermo Scientific) and its integrity was verified by agarose gel electrophoresis. After checking the integrity, 2 µg of the treated total RNA was used for cDNA synthesis using Maxima H Minus First Strand cDNA Synthesis Kit (Thermo Scientific, USA). Here random hexamers were used for first-strand cDNA synthesis following the manufacturer's protocol and these cDNA were used for real-time PCR analysis.

2.7. Quantitative real-time PCR analysis

The transcript profile of three key genes involved in the electron transfer of *R. sphaeroides* was analyzed. These genes included exopoly-saccharide production protein (exoY), Flp pilus assembly protein (tadD),

and cytochrome c oxidase, aa3 type, subunit I (coxI). Gene-specific primers were designed using primer3 - BLAST primer designing tool using default parameters (Table 1). The Recombinase gene (recA) was used as a housekeeping gene. Briefly, a 10 µL reaction was performed that includes 5 µL of 2X PowerUp SYBR Green Master Mix (Thermofisher Scientific, USA), 1 μ L each of forward and reverse primers (0.4 μ M), 1 μ L of cDNA template, and 2 µl of nuclease-free water. Reverse transcriptase PCR was performed using ABI PRISM® 7000 thermocycler QuantStudio 3 Real-Time PCR System (Applied Biosystems) following the manufacturer's protocol. The PCR program is as follows: UDG activation at 50 $^{\circ}\text{C}$ for 2 min; initial denaturation at 95 $^{\circ}$ C for 2 min using dual-lock DNA polymerase followed by 40 cycles of denaturation at 95 °C for 1 s and annealing at 60 °C for 30 s. Relative expression of the three genes was calculated using the $2^{-\Delta\Delta C_T}$ method (Livak and Schmittgen, 2001) using recombinase as the internal control gene for normalization. The experiment was performed in triplicates for each biological test sample. Nonspecific amplifications were checked using dissociation curves. No template control was also maintained throughout the experiment as a negative control without an RNA template.

2.8. Molecular docking studies

A 3 \times 3 nm 2D Gr-quantum dots structure was retrieved from the PubChem and optimized using universal force field (UFF) using the Avogadro software (Libavogadro Library, Pittsburgh, PA, USA). Molecular docking was carried out by the Discovery studio tool (Desault, US). Energy calculations using the docked site were visualized by CHIMERA (www.cgl.ucsf.edu/chimera) and PyMOL (http://pymol.sourceforge.net/) graphical tools.

3. Results and discussion

3.1. Electrode characterization

SEM analysis revealed the surface morphology of the CF and Ni/Gr electrodes used in this study. CF showed a ribbon-like structure with several grooves for bacterial cell adhesion and biofilm formation (Fig. 1a and e). Whereas, the Ni/Gr showed the exfoliated graphene layer on the signature honey-comb structure along with the grain boundaries (Fig. 1b and f). Raman spectra of Ni/Gr showed three prominent peaks (Fig. 1c). G peak at the Raman shift of 1574 cm⁻¹ represents the double degenerate zone center Raman active phonon E_{2g} mode of vibration. The 2D peak at the Raman shift of 2707 cm⁻¹ represents two phonon bands with twice electron scattering by transverse optical phonons (Lee et al., 2012). D peak at the Raman shift of 1330 cm⁻¹ represents the defect-induced band with electron scattering by the transverse optical phonon and a defect. It signifies the presence of defects on the graphene and the intensity implies a higher concentration of defects (Mafra et al., 2007; May et al., 2013).

The quantification of the defect and the number of layers can be evaluated by measuring the intensity ratios I_D/I_G and I_{2D}/I_G . The bare nickel foam did not show any prominent peaks and formed a smooth straight line in Raman spectra. The I_D/I_G and I_{2D}/I_G for CF was found to

Table 1Primer sets used for Reverse Transcriptase - quantitative Polymerase Chain Reaction (RT-qPCR) analysis.

Gene	Primer orientation	Sequence	PCR product size
exoY	Forward	GGCGCTACATCGACTATCCC	153 bp
exoY	Reverse	TCCAGTAGTTGTTCGCCGTC	
tadD	Forward	ACGAGACCTTCGAGCGTTAC	141 bp
tadD	Reverse	TCGAGAAGCCCCAGTTGTTC	
coxI	Forward	GGATGTCGACCGATCACCAG	166 bp
coxI	Reverse	ACTTCGCCCATCAGGTTCTG	
recA	Forward	GATCATGAAACTGGGGGCCA	187 bp
recA	Reverse	CTTCTTCTGCTCTTCCGCCA	

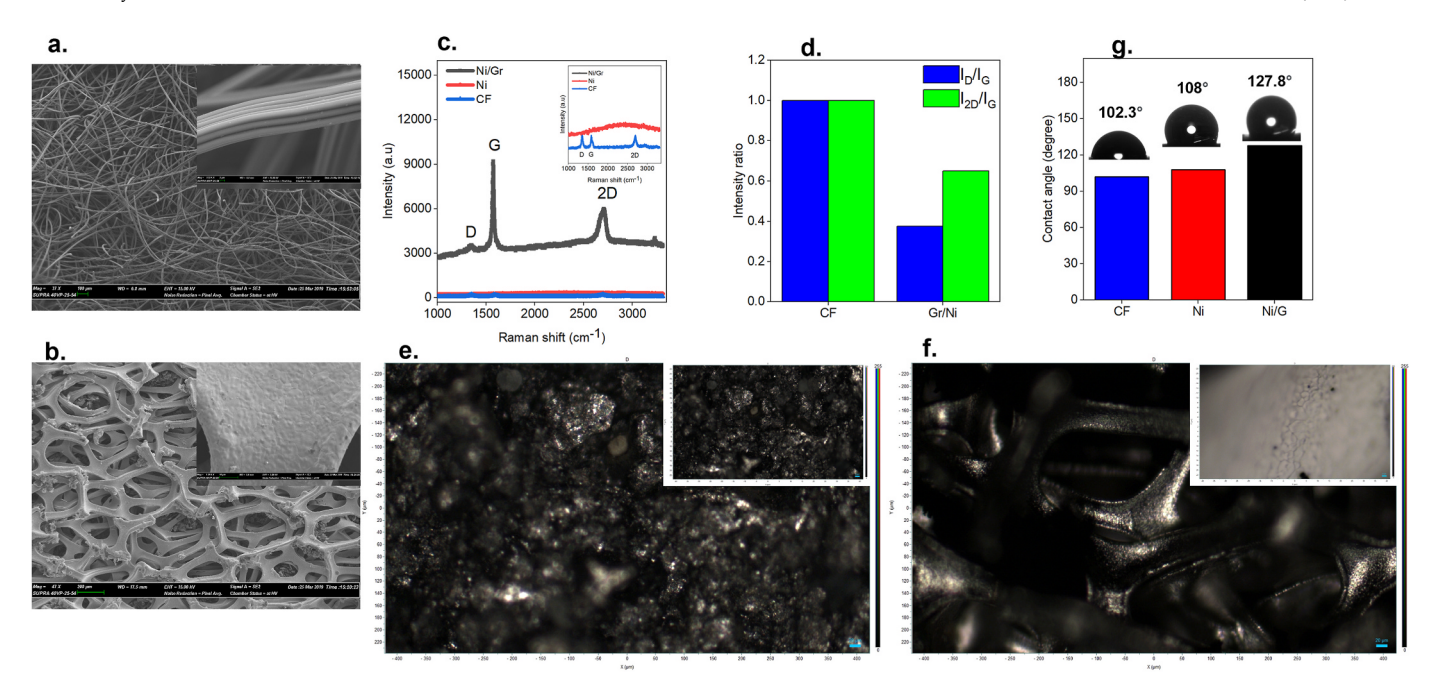


Fig. 1. Material characterization of Ni/Gr, Ni, and CF. 1a and 1b. SEM micrograph showing the ribbon-like structure of CF and Ni/Gr showing exfoliated graphene layer on Ni along with the grain boundaries. The inset figures are showing their higher magnifications. Several of these grooves favored bacterial cell adhesion and biofilm formation. 1c. Raman spectra showing the peak intensities of Ni/Gr, Ni, and CF. 1d. The ratios of the Raman peak intensities of $I_{D/G}$ and $I_{2D/G}$ of Ni/Gr, Ni, and CF. 1e and 1f. Light microscopic structures of Ni and Ni/Gr electrodes with inset showing at higher magnification. 1g. The static contact angle measurements of Ni/Gr, Ni, and CF electrodes used in this study.

be approximately 1 implying the presence of Carbon Nano Particle (CNPs) in non-crystalline graphite form. The sharp D and G peaks of CF represent the disordered graphite with possible clustering of $\rm sp^2$ phase and bond disorder (Boruah and Misra, 2016). However, the intensity ratio $\rm I_D/I_G$ of Ni/Gr below 0.4 and $\rm I_{2D}/I_G$ at approximately 0.6 (Fig. 1d) indicates the presence of few to multilayered graphene sheets deposited upon Nickel foam with high crystallinity but with the presence of few defects (Agudosi et al., 2020).

The Ni/Gr displayed 24.43% and 18.33% higher hydrophobicity (127.8°) than the conventional CF (102.3°) and bare nickel (108°) respectively (Fig. 1g). The subsequent electrochemical tests and gene expression studies revealed that the Ni/Gr showed enhanced electrochemical behavior and biofilm formation (see sections 3.2 and 3.4). This clearly shows that the more hydrophobic Ni/Gr influences the *R. sphaeroides* cell attachment, biofilm formation, and electricity production. This result corroborates the previous studies that hydrophobic electrodes are suitable for biofilm conditioning and electricity production (Liang et al., 2017; Pandit et al., 2017; Yang et al., 2015).

3.2. Bioelectrochemical interactions of R. sphaeroides cells with Ni/Gr

The pH was measured and found not to have any noticeable changes in the test and control pMFCs (Table 2). The bioelectrochemical interactions of *R. sphaeroides* with the Ni/Gr, and CF (control) surfaces in terms of pMFC performances were assessed (discussed below). The bare Ni yielded low OCV (0.2 V VS Ag/AgCl) and irreproducible performance. For example, the current output over time was inconsistent (not shown) and does not consider for further analysis. On the contrary, the Ni/Gr registered the OCV of 0.6 V and yielded a consistent current output of 513 μ A (Cycle I) and 443 μ A (Cycle II) overtime under closed-circuit conditions (150 Ω load) (see the i-t curve, Fig. 2a). The peak power output was 141 mW/m² and 88 mW/m² in Cycles I and II, respectively (Fig. 2b). Also, the temporal profile of the peak current densities were observed to be in the range of 15–55 and 233–620 mA m² in pMFC employing CF and Ni/Gr electrodes respectively (E-

 Table 2

 Summary of the R. sphaeroides performance in the three pMFCs.

Parameters		Electrodes in pMFC					
	Ni		CF		Ni/Gr		
	Cycle 1	Cycle 2	Cycle 1	Cycle 2	Cycle 1	Cycle 2	
Initial pH	7	7.1	7.1	7.1	7.1	7.1	
Final pH	6.8	6.9	6.9	7.0	7.0	7.0	
OCV (V)	0.2	0.21	0.29	0.2	0.6	0.58	
Peak power density (mW.m ⁻²)	9.8	1.2	8.6	1.6	141	88	
Peak current density (mA.m ⁻²)	83	31	59.5	15.2	620	584	

supplementary data Fig. S1). It is also noteworthy to mention that pMFC using Ni/Gr showed a maximum current density of 620 mA $\rm m^{-2}$ during 24 h incubation period whereas the CF electrode showed a maximum current density of 55 mA $\rm m^{-2}$ during 12 h incubation and declined further. Overall, these results reveal the phenomenal role of graphene layer on Ni in promoting the abilities of the *R. sphaeroides* cells at the biointerface. The results also show that the Ni/Gr electrodes are superior to the conventional carbon electrode (i.e., CF electrode).

The EIS results corroborate the findings from the pMFC polarization tests. The total resistance of Ni/Gr (0.005 Ω cm²) was 100-fold and 25-fold lower than bare Ni (0.53 Ω cm²) and CF (0.128), respectively (Fig. 3a, Table 3). The CV experiments at three different scan rates (10, 25, and 50 mV) showed the bio-catalytic performance by the presence of redox peak at -0.19 mV in Ni/Gr. In addition, the oxidation peak current in the Ni/Gr pMFC (0.0015 mA) was 2.1-folds higher than CF pMC (0.0007) respectively (Fig. 3c and d).

The COD removal rates for the CF and Ni/Gr ranged from 1211 to 963 mg/L and 1220-954 mg/L, respectively from the planktonic cells (Fig. 3b). This indicates that the biofilm cells might show tremendous exoelectrogenic cellular response to the electrodes than the planktonic cells, and thus biofilm is crucial for generating bioelectricity. The above

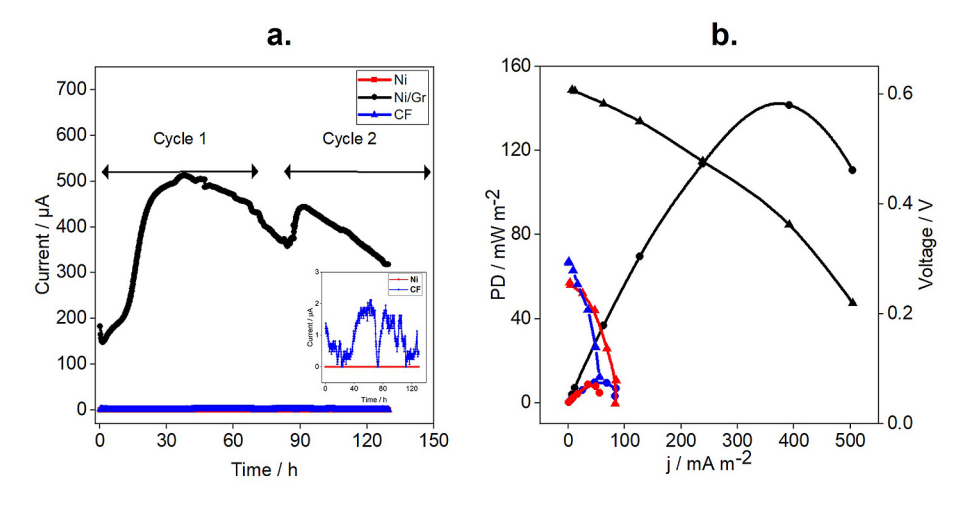
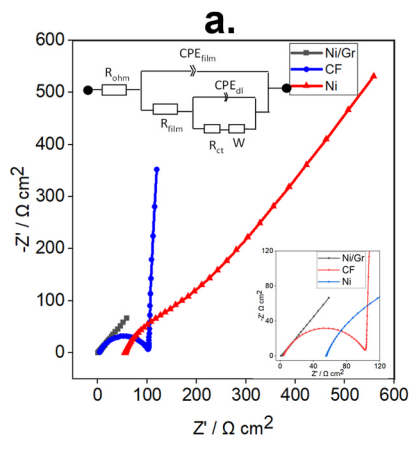


Fig. 2. Bioelectrochemical performances of *R. sphaeroides*. 2a. Temporal profile showing the current vs. time plot of *R. sphaeroides* pure cultures in pMFCs operated using CF (control), Ni/Gr, and Ni electrodes in two cycles. Inset shows the current vs. time plot for CF and Ni electrodes in pMFC. 2b. Polarization studies by comparing the power densities from the pMFC using Ni, CF, and Ni/Gr as electrodes. power densities (Ni), power densities (Ni/Gr), power densities (CF); voltage (Ni), voltage (Ni/Gr), voltage (CF).



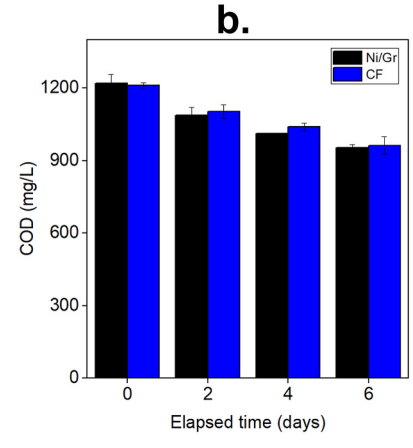
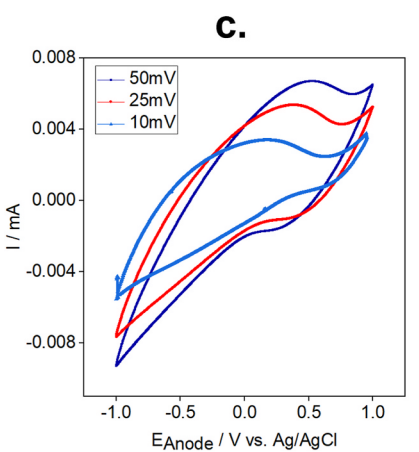
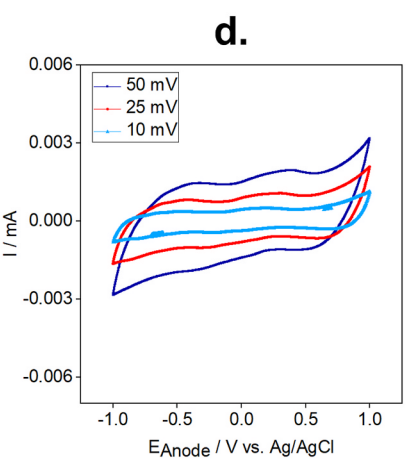


Fig. 3. EIS and cyclic voltammetry. 3a. Nyquist plots for Ni/Gr, Ni, and CF as anodes in pMFC. The inset plot shows a clear view of resistances offered at the *R. sphaeroides* electroactive biofilm on Ni and CF electrode material. **3b.** COD removal (mg/L) data of pMFCs incubated with Ni/Gr and CF electrodes. **3c.** CVs of pMFCs incubated with Ni/Gr electrode. **3d.** CVs of pMFCs incubated with CF electrode. The scan rates were 10, 25, and 50 mv/s, and the measurements were against Ag/AgCl reference electrode.





findings align with the previous reports on increased electrogenic activity (power density of 408 mW/m² and current density of 405 mA/cm²) of *R. sphaeroides* using graphite and platinum as the cathodic and anodic electrodes respectively (Cadirci, 2018). Also (Cho et al., 2008), reported a maximum power density of 790 mW/m² from *R. sphaeroides* grown in succinate/propionate and glutamate as carbon and nitrogen sources respectively using platinum-coated carbon paper anodes and cathodes. Furthermore, the electroactive-capacities of *R. sphaerodies* have been extensively reported using a variety of substrates including peptone (259 μ C); glucose, butyrate, malate, and fumarate (460–524 μ C); yeast extract (700 μ C); lactate and succinate (930–1007 μ C) as

electron donors wherein iron chelators along with nitrilotriacetic acid were found to mediate the EET to the electrodes (Wong et al., 2016). One of the existing limitations of MFCs is the high-cost platinum (metal catalyst) electrodes that are always a big hindrance for scale-up procedures (Pant et al., 2010) and thus non-platinized electrodes such as stainless steel or nickel alloys could be employed alternatively (Zhang et al., 2009).

To overcome the issues with lower power outputs, researchers developed graphene-based electrode materials to enhance the EET efficiency of microbes through functional group modification with added advantages including electrical/thermal conductivity, mechanical

Table 3 EIS fitting results show the various resistances in pMFCs - Ni, CF and Ni/Gr using *R. sphaeroides*. The total resistance of the electrode and electrolyte was found to be 0.533, 0.128 and 0.005 k Ω cm² for Ni, CF and Ni/Gr electrodes used in pMFC experiments respectively.

Resistances ^a	Ni	CF	Ni/Gr
R _{ohm} (kΩ. cm ²)	0.004	0.001	Negligible (0.1 \times 10 ⁻⁵)
R_{film} (k Ω . cm ²)	0.429	0.117	0.003
R_{ct} (k Ω . cm ²)	0.1	0.01	0.002
Total resistances	0.533	0.128	0.005

 $^{^{\}rm a}$ $R_{\rm ohm}$ - solution resistance; $R_{\rm film}$ – biofilm resistance; $R_{\rm ct}$ - charge transfer resistance

strength, lowest polarization resistance, good elasticity, and maximal specific surface area (Balandin et al., 2008; Kim et al., 2009; Lee et al., 2008; Stoller et al., 2008; Yuan and He, 2015). Improved EET was reported in Shewanella oneidensis using graphene oxide nanoribbon anodes that has large nanosized network structures resulting in the current density of $0.3~\mathrm{A~m^{-2}}$ and power density of $34.2~\mathrm{mW~m^{-2}}$ which were fourfold greater than their respective values with raw carbon paper anode used as a control (Huang et al., 2011). In another study, efficient EET in Shewanella spp. has been attributed due to the dense biofilm on electrodes apparently because of the enhanced direct electron transfer between the outer membrane c-type cytochromes and the anodes (Zou et al., 2016) along with the up-regulated expression of riboflavin biosynthesis enzyme (De Vriendt et al., 2005). Layer-by-layer assembly of graphene on carbon paper anode resulted in an increase of power density to 368 mW m⁻². These studies indicate that graphene materials improved the EET kinetics between the microbial outer membrane cytochromes and the electrode surfaces (Guo et al., 2014; Yu et al., 2016). Interestingly, a 3D reduced graphene oxide-nickel anode played a significant role in efficient EET in Shewanella oneidensis MR-1 resulting in an optimal volumetric power density of 661 W/m³ (Wang et al., 2013). Thus, in this study, Ni/Gr anode served as the best electron transfer coating for R. sphaeroides attachment and current generation along with the exceptional nickel skeleton. It is noteworthy to mention that the superior performance of the Ni/Gr anode is supposed to be due to several phenomena including the suitable surface area for microbial attachment, electron mediators, and high conductivity allowing for effective mass transfer of the electron donor/microbial growth medium. To the best of our knowledge, this is the first report on the Ni/Gr anode-based pMFC for the current generation using R. sphaeroides as the biocatalyst and CH₃OH as the electron donor.

3.3. Biofilm morphology of R. sphaeroides by SEM micrographs

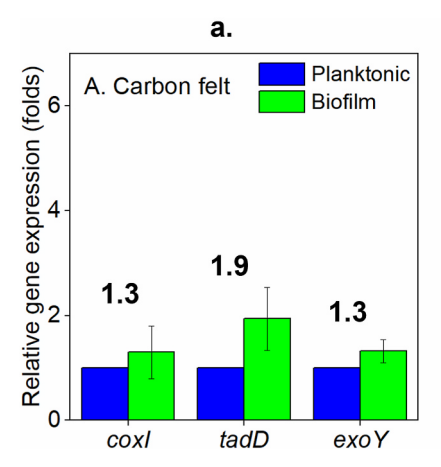
SEM micrographs showed that both Ni/Gr and CF served as a suitable electrodes for attachment and colonization of R. sphaeroides (E-Supplementary Figs. S2b and S2e). Also, the magnified images revealed loosely associated microbial clumps of rod-shaped bacterial cells with sizes ranging from 1 to 2 μm in length and ~500 nm in width (E-Supplementary Figs. S2c and S2f), which is consistent with the earlier reported morphological sizes of R. sphaeroides. Interestingly, R. sphaeroides cells grown on Ni/Gr electrodes were found to form an extensive biofilm than CF (E-Supplementary Fig. S2f). However, the control pMFCs without microbial inoculum using plain CF and Ni/Gr do not display any microbe biofilm (E-Supplementary Figs. S2a and S2d). This corroborates with the increased bioelectricity generation from R. sphaeroides grown on Ni/Gr anodes from the bioelectrochemical measurements (section 3.2). Also, the extremely high specific surface area of the Ni/Gr anode provided extensive microbial attachment and their outstanding electrical conductivity allowed enhanced electron transfer from the bacteria to the anodes (Chen et al., 2015). Biofilm formation of R. sphaeroides is highly determined by their specialized membrane phospholipid cardiolipin which plays a crucial role in the determination of cell shape,

biofilm formation, and its ability to adapt to the metabolically diverse environment (Lin et al., 2015, 2019). Although the exact genetic mechanism behind the *R. sphaeroides* biofilms is unexplored, essential flagellar genes including *FliA* and *FlgM* were reported to play a critical role as part of a complex regulatory network in flagellar synthesis, and the number of flagella per cell, motility, and biofilm formation (Wilkinson et al., 2011). Similar to this study, *Geobacter sulfurreducens* grown on titanium dioxide nanoparticles coated anode resulted in remarkably abundant pili formation than bare indium tin oxide control anode with a 5-fold increase in microbial current densities (Zhou et al., 2018). In addition, polyaniline hybridized 3D graphene electrode outperforms planar carbon electrode in MFC containing *Shewanella oneidensis* with enhanced EET efficiency and biofilm formation owing to the surface area of 3D graphene/PANI electrode and riboflavin molecules respectively (Yong et al., 2012).

The macro-porous structure of the 3D Ni/Gr increases the accessible surface area for bacterial attachment and subsequent stacking of sessile cells. Ni/Gr acted as an ideal electrochemically suitable material for the R. sphaeroides electroactive biofilm. Ni has been widely reported as an effective electrode material acting as a current collector (Zhang et al., 2009). This resulted in effective colonization of biofilm cells leading to the successful electroactive biofilm formation. Whereas in conventional electrodes like carbon felt, the thick diffusion-limited electrodic structure (Greenman et al., 2021) limited the biofilm attachment compared to Ni/Gr. Thus, plasma-exfoliated graphene on nickel-based electrodes not only offers a higher-surface area but also remains a suitable metall based electrodic platform for bioelectrochemical applications. These studies depict that electrochemical conductivity, and the 2D/3D structure of the anodes largely determine the microbial adhesion and biofilm formation on the MFC anodes. Thus, superconducting metallic Ni/Gr electrodes could very well serve as a good electron transfer layer for effective bio-electron transfer from the bacteria to the electrodes. In addition, this electrode has excellent mechanical properties with a flexible nickel skeleton which can be dented and folded into different shapes enabling them to fit into all types of MFCs (Wang et al., 2013). Moreover, the lightness of 3D anodes ensures higher specific power densities and an increase in thickness of these anodes could result in higher power outputs from MFCs (Yong et al., 2012). On another note, pMFCs could very well serve as a potential candidate for cheap and effective solar-based green energy resources (Cadirci, 2018).

3.4. Gene transcript profiling by RT-qPCR

The underlying molecular mechanisms involved in the exogenous electron transfer of R. sphaeroides to the electrodes and the biofilm formation are sparse. In this study, an effort was made to reveal insights into the key genes involved in EET and biofilm formation of R. sphaeroides grown in pMFC. Interestingly, RT-qPCR results showed that the candidate genes were differentially expressed in cells grown on Ni/Gr than CF anodes, calculated based on the cycle threshold values (Fig. 4). Cytochrome oxidase I (coxI) and pilus Flp pilus assembly protein (tadD) gene expressions were found to be moderately upregulated in the biofilm cells grown on CF by 1.3 \pm 0.5 folds and 1.9 \pm 0.6 folds (both insignificant) respectively (Fig. 4A). Whereas coxI and tadD genes were found to be significantly upregulated in the biofilm cells grown on Ni/Gr by 2.8 \pm 0.8 folds (P < 0.05) and 4.1 \pm 1.7 folds (P < 0.01) respectively (Fig. 4B). This indicates that these two genes play a crucial role in the EET and biofilm formation of R. sphaeroides exposed to the Ni/Gr electrodes. The exo Y gene transcripts of the biofilm on CF showed slight upregulation of 1.3 folds compared to planktonic cells. Interestingly, the exo Y gene expression on Ni/Gr biofilm was up-regulated significantly by 1.9 folds than planktonic cells. This shows that the $exo\ Y$ gene expression was moderately up-regulated in CF (1.3-folds) and significantly in Ni/Gr (1.9-folds) with high production of exopolysaccharides. Considering that the exo Y genes are regulatory proteins rather than structural components and thus they could be controlled by other factors



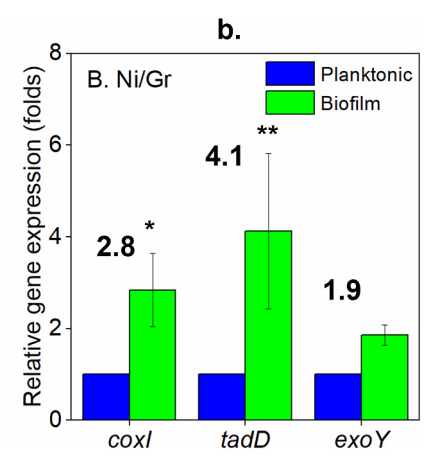


Fig. 4. Gene expression studies by RT-qPCR. 4a and 4b. Relative transcript abundance of genes encoding for *cox1* and *tadD* of planktonic and biofilm of *R. sphaeroides* in pMFC using CF **(4a)** and Ni/Gr **(4b)** anodes. Data represent the mean of the three independent biological repeats in which three technical triplicates were maintained each time for each gene. (Asterisk represents a significant difference **P < 0.01; *P < 0.05).

of genetic components. A mutant of *R. sphaeroides* that is deficient in cardiolipin synthase has been reported to inherit a similar exopoly-saccharide synthesis phenotype to control. This implies that several other genetic components of *R. sphaeroides* including cell growth, surface attachment, membrane permeability, swimming motility, and lipopolysaccharide synthesis are interrelated to exopolysaccharide synthesis (Lin et al., 2015). This corroborates the biocompatibility nature of Ni/Gr electrodes and their ability to promote the EET in this study. Owing to the lower conductivity, the CF electrode yielded poor performance.

Photosynthetically grown R. sphaeroides synthesize intracytoplasmic membrane (ICM) which possesses the structural components that are essential for photosynthetic light energy capture, electron transport machinery, and energy transduction (Roh et al., 2004). The ubiquinone pool of R. sphaeroides has been reported to play a critical role in the endogenous electron fluxes from the central metabolism directing towards various electron dissipation pathways. Whereas the iron chelator along with nitrilotriacetic acid served as a mediator for shuttling electrons from the intracellular environment of R. sphaeroides to the electrodes (Wong et al., 2016). However, the precise EET mechanism of R. sphaeroides has not been reported so far. Therefore, it is rational to propose that abundant EPS formation on Ni/Gr anodes was likely responsible for the enhanced electrochemical conductivity of R. sphaeroides. Further studies including transcriptomic analysis revealing the RNA transcript levels and their enriched gene ontologies along with gene clustering analysis of the entire transcriptome could be performed to reveal the exact mechanism of EET in R. sphaeroides. Also, integrated knowledge of bioelectrochemistry, isotope-assisted phylogeny, transcriptomics, and proteomic analysis could provide further breakthroughs toward augmenting enhanced power generation from microorganisms using MFCs (Choudhury et al., 2017).

3.5. Potential pathways of electron transfer in R. sphaeroides

The biochemical pathways of the *R. sphaeroides* have been previously reported only under specific environmental conditions. The current study explored photosynthetic electron transfer pathways of this species to insoluble electron acceptors (i.e.,electrodes in microbial fuel cells) a. The competing pathways involved in cytoplasmic quinone pool mediated electron transfer of *R. sphaeroides* have been previously identified as PHB synthesis, hydrogen production, and light-harvesting complex metabolism (Wong et al., 2016). A heterologous expression of multi-heme protein complex MtrCAB has also been performed, that implicates the feasibility of redirecting the endogenous electrons to the extracellular electron pathway through synthetic biology (Cheng et al.,

2013). Alhough R. sphaeroides has been evaluated for bioelectrochemical applications (Cadirci, 2018; Cho et al., 2008; Jawaharraj et al., 2020b; Rosenbaum et al., 2005; Wong et al., 2016; Wong and Tung, 2015), the exact mechanism of the photosynthetic electron transfer has not been well elucidated. Here, a photosynthetic CH₃OH oxidation pathway of R. sphaeroides that drives endogenous electrons to nickel electrodes modified with graphene was analyzed. Four major components including quinone pool, cytochrome-c, cbb3 Cyt-C oxidases along with membrane proteins and symporters contributed to the EET potential of *R. sphaeroides* grown on the Ni/Gr electrodes. Cytochrome *c* oxidase and cardiolipin have also been reported to play a major role in the cellular morphology and biofilm formation (Lin et al., 2015, 2019). Here, four thermodynamically stable conformations of the cytochrome-graphene surface were observed, and the efficient electron transfer was dependent upon both the position of the heme group and its relative orientation with graphene (Kowalska et al., 2018). Multi-heme c-type cytochrome complexes are also vital outer membrane proteins involved in the EET in electroactive biofilms (Chatterjee et al., 2021).

Also, MD simulations revealed molecular interactions of GO nanosheets with the cytochrome protein, which is crucial for EET in an electroactive biofilm (Supplementary Fig. S3). The crystallographic structure of the Cytochrome-C (Cyt-C) core component (PDB ID 2GSM) was obtained from the online Research Collaboratory for Structural Bioinformatics Protein Data Bank (http://www.pdb.org). Molecular docking was performed with an optimized 2D graphene sheet. The interacting site was visualized after optimizing the protein structure. The GO nanosheet with interacting residues within 4 Å and the spatial conformation in the binding site are depicted in Supplementary Fig. S3. The nearest interacting residues are Thr, Ser, Val, Glu, and Asn. In-silico studies confirmed that the graphene sheet served as a conducting material and interacted with the subunit-C of the cytochrome-C (Cyt-C) core complex. With the 3D conformation of the core complex and due to the spatial arrangement of the protein, the Gr-sheet resides within the narrow gap that exists within the Cyt-C. However, the absence of the functional groups results in minimal interactions with the subunit-C. Our gene transcript analysis by real-time PCR also corroborates with the MD simulation study showing elevated levels of cytochrome gene expression when grown using graphene exfoliated nickel electrodes than conventional carbon electrodes. Besides a well-established quorum sensing pathway was reported in R. sphaeroides that produces acylhomoserine lactone (AHL) molecules that regulates the electroactive biofilms. R. sphaeroides harbors community escape response (cer) genes such as cerI and cerR that regulate the secretion of a novel AHL molecule 7,8-cis-N-(tetradecenoyl) homoserine lactone which is crucial for biofilm formation and quorum sensing (QS) signaling pathway (Puskas et al., 1997). This pathway allows the bacterial system to monitor the population density and trigger specific *cer* genes at necessarily high cell numbers. Deletion of *cerI* gene in *R. sphaeroides* resulted in the differential phenotype of mucoid colony formation in agar medium and large aggregates in liquid medium. Presumably, the overproduction of extracellular polysaccharides among the *cerI* mutants could be the reason for the large cell aggregates and mucoid colony phenotypes (Puskas et al., 1997). On the other hand, research on regulating the electron inflow and outflow of *R. sphaeroides* is warranted to maximize the EET in bioelectrochemical fuel cells (Wong et al., 2016). The current study revealed the evidence of surface-modified graphene-based electrodes could efficiently increase the electroactive potential of photosynthetic microbe grown in microbial fuel cells. Future research is warranted to study the genotypic and phenotypic biomolecular regulations behind this enhanced electroactive biofilm formation.

4. Conclusion

This study serves as proof-of-concept for using graphene coated nickel electrodes for enabling methylotrophs as microbial cell factories, specifically for treating the anaerobic industrial wastewaters dominated by CH₃OH. This study demonstrates the use of graphene layers as minimally invasive coatings for improving the bioelectrochemical interactions of *R. sphaeroides* cells with underlying ferromagnetic nickel surfaces in CH₃OH-based pMFCs. The improved interactions were evident from the increased current from CH₃OH oxidation, upregulation of the candidate genes involved in electron transfer, and the improved electroactive ability of *R. sphaeroides* cells to attach and form electrogenic biofilms on nickel surfaces. Omics studies are warranted to establish genome-phenome relationships of the *R. sphaeroides* cells grown on nickel electrodes. Further studies are also required to assess the feasibility of modifying diamagnetic metals such as copper with graphene for subsequent use in photosynthetic MFCS.

Credit author statement

Kalimuthu Jawaharraj: Resources, Conceptualization, Visualization, and Validation. Pawan Sigdel: Validation. Zhengrong Gu: Resources. Govarthanan Muthusamy: Validation. Rajesh Sani: Project administration. Venkataramana Gadhamshetty: Resources, Conceptualization, Supervision, Validation, Project administration, Funding acquisition.

Declaration of competing interest

The authors declare that they have no known competing financial interests or personal relationships that could have appeared to influence the work reported in this paper.

Data availability

Data will be made available on request.

Acknowledgments

The authors acknowledge the funding support from National Science Foundation, United States (Awards#1849206, #1920954, #1736255) and National Aeronautics and Space Administration, United States (#NNX16AQ98A).

Appendix A. Supplementary data

Supplementary data to this article can be found online at https://doi. org/10.1016/j.envres.2022.114045.

References

- Agudosi, E.S., Abdullah, E.C., Numan, A., Mubarak, N.M., Aid, S.R., Benages-Vilau, R., Gómez-Romero, P., Khalid, M., Omar, N., 2020. Fabrication of 3D binder-free graphene NiO electrode for highly stable supercapattery. Sci. Rep. 10, 1–13. https:// doi.org/10.1038/s41598-020-68067-2.
- Balandin, A.A., Ghosh, S., Bao, W., Calizo, I., Teweldebrhan, D., Miao, F., Lau, C.N., 2008. Superior thermal conductivity of single-layer graphene. Nano Lett. 8, 902–907. https://doi.org/10.1021/nl0731872.
- Boruah, B.D., Misra, A., 2016. Nickel hydroxide coated carbon nanoparticles mediated hybrid three-dimensional graphene foam assembly for supercapacitor. RSC Adv. 6, 36307–36313. https://doi.org/10.1039/c6ra04918d.
- Bowman, J., Sayler, G., 1994. Optimization and maintenance of soluble methane monooxygenase activity in *Methylosinus trichosporium* OB3b, 1994 Mar Biodegradation 5 (1), 1–11. https://doi.org/10.1007/BF00695208, 10.1007/ BF00695208, PMID 7764924, 1, 7764924.
- Cadirci, B.H., 2018. An electricity production study by *Rhodobacter sphaeroides*. Int. J. Hydrogen Energy 43, 18001–18006. https://doi.org/10.1016/j. iihydene.2018.01.146.
- Cai, M., An, C., Guy, C., Lu, C., Mafakheri, F., 2021. Assessing the regional biogenic methanol emission from spring wheat during the growing season: a Canadian case and Province Polluty 2021, 1175(2).
- study. Environ. Pollut. 287, 117602 https://doi.org/10.1016/j.envpol.2021.117602. Chatterjee, M., Fan, Y., Cao, F., Jones, A.A., Pilloni, G., Zhang, X., 2021. Proteomic study of *Desulfovibrio ferrophilus* 1S5 reveals overexpressed extracellular multi-heme cytochrome associated with severe microbiologically influenced corrosion. Sci. Rep. 11. 1–11. https://doi.org/10.1038/s41598-021-95060-0.
- Chen, J., Deng, F., Hu, Y., Sun, J., Yang, Y., 2015. Antibacterial activity of graphene-modified anode on *Shewanella oneidensis* MR-1 biofilm in microbial fuel cell. J. Power Sources 290, 80–86. https://doi.org/10.1016/j.jpowsour.2015.03.033.
- Cheng, D., Wang, W., Chow, K., Hsing, I.-M., 2013. Engineering Rhodobacter sphaeroides for direct electron transfer by heterogenous expression of redox-active components from electrogenic species. In: 2013 AIChE Annual Meeting, San Francisco, CA, USA, 3-8 November. International Union of Microbiological Societies Congresses, IUMS 2014.
- Chilkoor, G., Sarde, R., Islam, J., ArunKumar, K.E., Ratnayake, I., Star, S., Jasthi, B.K., Sereda, G., Koratkar, N., Meyyappan, M., G. V, 2020. Maleic anhydride-functionalized graphene nanofillers render epoxy coatings highly resistant to corrosion and microbial attack. Carbon N. Y. https://doi.org/10.1016/j.carbon 2019 12 059
- Chilkoor, G., Shrestha, N., Kutana, A., Tripathi, M., Robles Hernández, F.C., Yakobson, B. I., Meyyappan, M., Dalton, A.B., Ajayan, P.M., Rahman, M.M., Gadhamshetty, V., 2021. Atomic layers of graphene for microbial corrosion prevention. ACS Nano 15, 447–454. https://doi.org/10.1021/acsnano.0c03987.
- Cho, Y.K., Donohue, T.J., Tejedor, I., Anderson, M.A., McMahon, K.D., Noguera, D.R., 2008. Development of a solar-powered microbial fuel cell. J. Appl. Microbiol. 104, 640–650. https://doi.org/10.1111/j.1365-2672.2007.03580.x.
- Choudhury, A., Barbora, L., Arya, D., Lal, B., Subudhi, S., Mohan, S.V., Ahammad, S.Z., Verma, A., 2017. Effect of electrode surface properties on enhanced electron transfer activity in microbial fuel cells. Eng. Life Sci. 17, 186–192. https://doi.org/10.1002/elsc.201600063.
- De Vriendt, K., Theunissen, S., Carpentier, W., De Smet, L., Devreese, B., Van Beeumen, J., 2005. Proteomics of *Shewanella oneidensis* MR-1 biofilm reveals differentially expressed proteins, including AggA and RibB. Proteomics 5, 1308–1316. https://doi.org/10.1002/pmic.200400989.
- Dedysh, S.N., Didriksen, A., Danilova, O.V., Belova, S.E., Liebner, S., Svenning, M.M., 2015. *Methylocapsa palsarum* sp. nov., a methanotroph isolated from a subarctic discontinuous permafrost ecosystem. Int. J. Syst. Evol. Microbiol. 65, 3618–3624. https://doi.org/10.1099/ijsem.0.000465.
- EPA, 2004. US Environmental Protection Agency, US EPA. Toxics Release Inventory (TRI). www.epa.gov/tri. accessed 10.07.04.
- EPA, 1998. US Environmental Protection Agency, National emission standards for hazardous air pollutants for source category: Pulp and paper production; Effluent limitations guidelines, pretreatment standards, and new source performance standards: Pulp, Paper, and Paperboard Category, 63, 18504–18751.
- Greenman, J., Gajda, I., You, J., Mendis, B.A., Obata, O., Pasternak, G., Ieropoulos, I., 2021. Microbial fuel cells and their electrified biofilms. Biofilm 20 (3), 100057. https://doi.org/10.1016/j.biofim.2021.100057.
- Guo, W., Cui, Y., Song, H., Sun, J., 2014. Layer-by-layer construction of graphene-based microbial fuel cell for improved power generation and methyl orange removal. Bioproc. Biosyst. Eng. 37, 1749–1758. https://doi.org/10.1007/s00449-014-1148-y.
- Huang, W., Wang, H., Zhou, J., Wang, J., Duchesne, P.N., Muir, D., Zhang, P., Han, N., Zhao, F., Zeng, M., Zhong, J., Jin, C., Li, Y., Lee, S.T., Dai, H., 2015. Highly active and durable methanol oxidation electrocatalyst based on the synergy of platinum-nickel hydroxide-graphene. Nat. Commun. 6, 1–8. https://doi.org/10.1038/ncomms10035.
- Huang, Y.X., Liu, X.W., Xie, J.F., Sheng, G.P., Wang, G.Y., Zhang, Y.Y., Xu, A.W., Yu, H. Q., 2011. Graphene oxide nanoribbons greatly enhance extracellular electron transfer in bio-electrochemical systems. Chem. Commun. 47, 5795–5797. https://doi.org/10.1039/c1cc10159e.
- Hummers Jr., W.S., Offeman, R.E., 1958. Preparation of graphitic oxide. J. Am. Chem. Soc. 80, 1339.
- Islam, J., Chilkoor, G., Jawaharraj, K., Dhiman, S.S., Sani, R., Gadhamshetty, V., 2020. Vitamin-C-enabled reduced graphene oxide chemistry for tuning biofilm phenotypes of methylotrophs on nickel electrodes in microbial fuel cells. Bioresour. Technol. 300, 122642 https://doi.org/10.1016/j.biortech.2019.122642.

- Jawaharraj, K., Gadhamshetty, V., Vemuri, B., Islam, J., Dhiman, S., Sani, R., 2019. Extracellular electron transfer capabilities of phenotypically improved methylotrophs. In: SIMB Annual Meeting and Exhibition 2019.
- Jawaharraj, K., Shrestha, N., Chilkoor, G., Dhiman, S.S., Islam, J., Gadhamshetty, V., 2020a. Valorization of methane from environmental engineering applications: a critical review. Water Res. 187, 116400 https://doi.org/10.1016/j. watres.2020.116400.
- Jawaharraj, K., Shrestha, N., Chilkoor, G., Vemuri, B., Gadhamshetty, V., 2020b. Electricity from methanol using indigenous methylotrophs from hydraulic fracturing flowback water. Bioelectrochemistry 135, 107549. https://doi.org/10.1016/j. bioelechem.2020.107549.
- Jawaharraj, K., Sudha Dhiman, S., Bedwell, S., Vemuri, B., Islam, J., Sani, R.K., Gadhamshetty, V., 2021. Electricity from methane by *Methylococcus capsulatus* (Bath) and *Methylosinus trichosporium* OB3b. Bioresour. Technol. 321 https://doi. org/10.1016/j.biortech.2020.124398.
- Kaur, R., Marwaha, A., Chhabra, V.A., Kim, K.H., Tripathi, S.K., 2020. Recent developments on functional nanomaterial-based electrodes for microbial fuel cells. Renew. Sustain. Energy Rev. 119, 109551 https://doi.org/10.1016/j. resr 2019 109551
- Kim, Keun Soo, Zhao, Y., Jang, H., Lee, S.Y., Kim, J.M., Kim, Kwang S., Ahn, J.H., Kim, P., Choi, J.Y., Hong, B.H., 2009. Large-scale pattern growth of graphene films for stretchable transparent electrodes. Nature 457, 706–710. https://doi.org/ 10.1038/nature07719.
- Kowalska, A.M., Trzaskowski, B., Osella, S., 2018. Assessing the charge transfer at the cytochrome c553/graphene interface: a multiscale investigation. J. Phys. Chem. C 122, 29405–29413. https://doi.org/10.1021/acs.jpcc.8b10517.
- Krishnamurthy, A., Gadhamshetty, V., Mukherjee, R., Chen, Z., Ren, W., Cheng, H.M., Koratkar, N., 2013. Passivation of microbial corrosion using a graphene coating. Carbon N. Y. 56, 45–49. https://doi.org/10.1016/j.carbon.2012.12.060.
- Langrand, G., Rondot, N., Triantaphylides, C., Baratti, J., 1990. Short chain flavour esters synthesis by microbial lipases. Biotechnol. Lett. 12, 581–586. https://doi.org/ 10.1007/BF01030756.
- Lee, C., Wei, X., Kysar, J.W., Hone, J., 2008. Measurement of the elastic properties and intrinsic strength of monolayer graphene. Science 321 (80), 385–388. https://doi. org/10.1126/science.1157996.
- Lee, J.E., Ahn, G., Shim, J., Lee, Y.S., Ryu, S., 2012. Optical separation of mechanical strain from charge doping in graphene. Nat. Commun. 3 https://doi.org/10.1038/pcomms/2022
- Li, S., Sakuntala, M., Song, Y.E., Heo, J. ook, Kim, M., Lee, S.Y., Kim, M.S., Oh, Y.K., Kim, J.R., 2021. Photoautotrophic hydrogen production of *Rhodobacter sphaeroides* in a microbial electrosynthesis cell. Bioresour. Technol. 320, 124333 https://doi. org/10.1016/j.biortech.2020.124333.
- Liang, Y., Feng, H., Shen, D., Li, N., Guo, K., Zhou, Y., Xu, J., Chen, W., Jia, Y., Huang, B., 2017. Enhancement of anodic biofilm formation and current output in microbial fuel cells by composite modification of stainless steel electrodes. J. Power Sources 342, 98–104. https://doi.org/10.1016/j.jpowsour.2016.12.020.
- Lin, T.Y., Gross, W.S., Auer, G.K., Weibel, D.B., 2019. Cardiolipin alters *Rhodobacter sphaeroides* cell shape by affecting peptidoglycan precursor biosynthesis. mBio 10. https://doi.org/10.1128/mBio.02401-18.
- Lin, T.Y., Santos, T.M.A., Kontur, W.S., Donohue, T.J., Weibel, D.B., 2015. A cardiolipin-deficient mutant of *Rhodobacter sphaeroides* has an altered cell shape and is impaired in biofilm formation. J. Bacteriol. 197, 3446–3455. https://doi.org/10.1128/ IB 00420-15
- Livak, K.J., Schmittgen, T.D., 2001. Analysis of relative gene expression data using real-time quantitative PCR and the 2^{·ΔΔC_T} method. Methods 25, 402–408. https://doi.org/10.1006/meth.2001.1262.
- Maddalwar, S., Kumar Nayak, K., Kumar, M., Singh, L., 2021. Plant microbial fuel cell: opportunities, challenges, and prospects. Bioresour. Technol. 341, 125772 https://doi.org/10.1016/j.biortech.2021.125772.
- Mafra, D.L., Samsonidze, G., Malard, L.M., Elias, D.C., Brant, J.C., Plentz, F., Alves, E.S., Pimenta, M.A., 2007. Determination of LA and TO phonon dispersion relations of graphene near the Dirac point by double resonance Raman scattering. Phys. Rev. B Condens. Matter 76, 3–6. https://doi.org/10.1103/PhysRevB.76.233407.
- May, P., Lazzeri, M., Venezuela, P., Herziger, F., Callsen, G., Reparaz, J.S., Hoffmann, A., Mauri, F., Maultzsch, J., 2013. Signature of the two-dimensional phonon dispersion in graphene probed by double-resonant Raman scattering. Phys. Rev. B Condens. Matter 87, 1–6. https://doi.org/10.1103/PhysRevB.87.075402.
- Mirza, S.S., Al-Ansari, M.M., Ali, M., Aslam, S., Akmal, M., Al-Humaid, L., Hussain, A., 2022. Towards sustainable wastewater treatment: influence of iron, zinc and aluminum as anode in combination with salt bridge on microbial fuel cell performance. Environ. Res. 209, 112781 https://doi.org/10.1016/J. ENVRES.2022.112781.
- Pandit, S., Shanbhag, S., Mauter, M., Oren, Y., Herzberg, M., 2017. Influence of electric fields on biofouling of carbonaceous electrodes. Environ. Sci. Technol. 51, 10022–10030. https://doi.org/10.1021/acs.est.6b06339.
- Pant, D., Van Bogaert, G., Diels, L., Vanbroekhoven, K., 2010. A review of the substrates used in microbial fuel cells (MFCs) for sustainable energy production. Bioresour. Technol. 101, 1533–1543. https://doi.org/10.1016/j.biortech.2009.10.017.
- Puskas, A., Greenberg, E.P., Kaplan, S., Schaefer, A.L., 1997. A quorum-sensing system in the free-living photosynthetic bacterium *Rhodobacter sphaeroides*. J. Bacteriol. 179, 7530–7537. https://doi.org/10.1128/jb.179.23.7530-7537.1997.
- Qi, X., Ren, Y., Liang, P., Wang, X., 2018. New insights in photosynthetic microbial fuel cell using anoxygenic phototrophic bacteria. Bioresour. Technol. 258, 310–317. https://doi.org/10.1016/j.biortech.2018.03.058.
- Roh, J.H., Smith, W.E., Kaplan, S., 2004. Effects of oxygen and light intensity on transcriptome expression in *Rhodobacter sphaeroides* 2.4.1: redox active gene

- expression profile. J. Biol. Chem. 279, 9146–9155. https://doi.org/10.1074/jbc. M311608200.
- Rosenbaum, M., Schröder, U., Scholz, F., 2005. In situ electrooxidation of photobiological hydrogen in a photobioelectrochemical fuel cell based on *Rhodobacter sphaeroides*. Environ. Sci. Technol. 39, 6328–6333. https://doi.org/10.1021/es0505447.
- Roy, J.N., Luckarift, H.R., Lau, C., Falase, A., Garcia, K.E., Ista, L.K., Chellamuthu, P., Ramasamy, R.P., Gadhamshetty, V., Wanger, G., Gorby, Y.A., 2012. A study of the flavin response by *Shewanella* cultures in carbon-limited environments. RSC Adv. 2 (26), 10020–10027.
- Shrestha, N., Chilkoor, G., Wilder, J., Ren, Z.J., Gadhamshetty, V., 2018. Comparative performances of microbial capacitive deionization cell and microbial fuel cell fed with produced water from the Bakken shale. Bioelectrochemistry 121, 56–64. https://doi.org/10.1016/j.bioelechem.2018.01.004.
- Shrestha, N., Fogg, A., Wilder, J., Franco, D., Komisar, S., Gadhamshetty, V., 2016. Electricity generation from defective tomatoes. Bioelectrochemistry 112, 67–76. https://doi.org/10.1016/j.bioelechem.2016.07.005.
- Statista, 2022. Water and wastewater treatment market size worldwide in 2020, with a forecast to 2028(in billion U.S. dollars) [WWW Document]. https://www.statista.com/statistics/1199744/market-size-water-and-wastewater-treatment-global/.
- Stoller, M.D., Park, S., Zhu, Y., An, J., Ruoff, R.S., 2008. Graphene-based ultracapacitors. Nano Lett. 6–10.
- Swain, H.M., Somerville, H.J., 1978. Microbial metabolism of methanol in a model activated sludge system. J. Appl. Bacteriol. 45, 147–151. https://doi.org/10.1111/ j.1365-2672.1978.tb04209.x.
- Tchobanoglus, G., Burton, F., Stensel, H.D., 2003. Wastewater engineering: treatment and reuse. Am. Water Works Assoc. J. 95, 201.
- Tripathi, A.K., Thakur, P., Saxena, P., Rauniyar, S., Gopalakrishnan, V., Singh, R.N., Gadhamshetty, V., Gnimpieba, E.Z., Jasthi, B.K., Sani, R.K., 2021. Gene sets and mechanisms of sulfate-reducing bacteria biofilm formation and quorum sensing with impact on corrosion. Front. Microbiol. 29 (12), 754140 https://doi.org/10.3389/fmicb.2021.754140.
- Wang, H., Wang, G., Ling, Y., Qian, F., Song, Y., Lu, X., Chen, S., Tong, Y., Li, Y., 2013. High power density microbial fuel cell with flexible 3D graphene-nickel foam as anode. Nanoscale 5, 10283–10290. https://doi.org/10.1039/c3nr03487a.
- Wang, K., Xu, M., Gu, Y., Gu, Z., Liu, J., Fan, Q.H., 2017. Low-temperature plasma exfoliated n-doped graphene for symmetrical electrode supercapacitors. Nano Energy 31, 486–494. https://doi.org/10.1016/j.nanoen.2016.11.007.
- Wilkinson, D.A., Chacko, S.J., Vénien-Bryan, C., Wadhams, G.H., Armitage, J.P., 2011. Regulation of flagellum number by FliA and FlgM and role in biofilm formation by Rhodobacter sphaeroides. J. Bacteriol. 193, 4010–4014. https://doi.org/10.1128/ JB.00349-11.
- Wilson, S.M., Gleisten, M.P., Donohue, T.J., 2008. Identification of proteins involved in formaldehyde metabolism by Rhodobacter sphaeroides. Microbiology 154, 296–305.
- Wong, M.T., Cheng, D., Wang, R., Hsing, I.M., 2016. Modifying the endogenous electron fluxes of *Rhodobacter sphaeroides* 2.4.1 for improved electricity generation. Enzym. Microb. Technol. 86, 45–51. https://doi.org/10.1016/j.enzmictec.2016.01.009.
- Wong, Tung, M., 2015. Utilization and characterization of photosynthetic bacteria *rhodobacter sphaeroides* for bioelectricity generation. Thesis (M.Phil.), 2015. Hong Kong University of Science and Technology.
 Y, T., T, Y., Y., S., Bd, Y., 1987. Microbiological synthesis from C1-compounds:
- Y, T., T, Y., Y, S., Bd, Y., 1987. Microbiological synthesis from C1-compounds: application of some methylotrophic functions to synthesis of useful chemicals. In: Van Verseveld, H.W., Duine, J.A. (Eds.), Microbial Growth on C1 Compounds, Proceedings of the 5th International Symposium. Martinus Nijhoff Publishers, np. 282–288
- Yamamuro, A., Kouzuma, A., Abe, T., Watanabe, K., 2014. Metagenomic analyses reveal the involvement of syntrophic consortia in methanol/electricity conversion in microbial fuel cells. PLoS One 9, 1–8. https://doi.org/10.1371/journal. pone.0098425.
- Yang, Y., Wu, Y., Hu, Y., Cao, Y., Poh, C.L., Cao, B., Song, H., 2015. Engineering electrode-attached microbial consortia for high-performance xylose-fed microbial fuel cell. ACS Catal. 5, 6937–6945. https://doi.org/10.1021/acscatal.5b01733.
- Yaqoob, A.A., Ibrahim, M.N.M., Rodríguez-Couto, S., 2020. Development and modification of materials to build cost-effective anodes for microbial fuel cells (MFCs): an overview. Biochem. Eng. J. 164, 107779 https://doi.org/10.1016/j. bej.2020.107779.
- Yong, Y.C., Dong, X.C., Chan-Park, M.B., Song, H., Chen, P., 2012. Macroporous and monolithic anode based on polyaniline hybridized three-dimensional Graphene for high-performance microbial fuel cells. ACS Nano 6, 2394–2400. https://doi.org/ 10.1021/nn204656d.
- Yu, F., Wang, C., Ma, J., 2016. Applications of graphene-modified electrodes in microbial fuel cells. Materials 9. https://doi.org/10.3390/ma9100807.
- Yuan, H., He, Z., 2015. Graphene-modified electrodes for enhancing the performance of microbial fuel cells. Nanoscale 7, 7022–7029. https://doi.org/10.1039/c4nr05637j.
- Zhang, F., Cheng, S., Pant, D., Bogaert, G. Van, Logan, B.E., 2009. Power generation using an activated carbon and metal mesh cathode in a microbial fuel cell. Electrochem. Commun. 11, 2177–2179. https://doi.org/10.1016/j.elecom.2009.09.024.
- Zhou, S., Tang, J., Yuan, Y., Yang, G., Xing, B., 2018. TiO₂ nanoparticle-induced nanowire formation facilitates extracellular electron transfer. Environ. Sci. Technol. Lett. 5, 564–570. https://doi.org/10.1021/acs.estlett.8b00275.
- Zou, L., Qiao, Y., Wu, X.S., Li, C.M., 2016. Tailoring hierarchically porous graphene architecture by carbon nanotube to accelerate extracellular electron transfer of anodic biofilm in microbial fuel cells. J. Power Sources 328, 143–150. https://doi. org/10.1016/j.jpowsour.2016.08.009.